ELSEVIER

Polymer 41 (2000) 4643–4649

polymer

Low-, stray-field imaging and spectroscopic studies of the sodium polyacrylate water uptake

T.G. Nunes[a,*], G. Guillot[c], J.M. Bordado[c]

[a]*ICTPOL/IST, Departamento de Engenharia de Materiais, Av. Rovisco Pais, 1, 1049-001 Lisbon, Portugal*
[b]*Unité de Recherche en RM Médicale, CNRS ESA 8081, Bât. 220, U.P.S. F91405 Orsay Cedex, France*
[c]*Hoechst Portuguesa, R&D, Apt. 6, 2726 Mem Martins, Portugal*

Received 31 May 1999; received in revised form 30 July 1999; accepted 6 August 1999

Abstract

Water uptake in sodium polyacrylate was followed by low-field magnetic resonance imaging (LF-MRI), at 0.1 T and 5 mT/m, and by stray-field magnetic resonance imaging (STRAFI-MRI), at 2.9 T and 37.5 T/m, over 50 h. One-dimensional (1-D) images were recorded and the model for the diffusion of the liquid into the polymer was obtained. The complementarity of the techniques is discussed. ^{1}H, ^{13}C and ^{23}Na spectroscopic NMR data are also presented.

Keywords: Sodium polyacrylate; Water uptake; NMR

1. Introduction

Water uptake is an important property to be evaluated, especially if the materials are designed to function in aqueous environments. Water uptake is generally monitored by gravimetric analysis of the material, in which case no information on the spatial variation of the migration kinetics is obtained. Magnetic resonance imaging (MRI) has proven to be a powerful technique to provide spin-density maps of water diffusing into polymeric materials.

Polymer-penetrant systems exhibit a large range of diffusion phenomena, from a common Fickian (or Case I) diffusion to Case II diffusion, which represent the two extreme diffusion behaviours, according to Alfrey et al. [1]. In general, Case I applies to amorphous polymers *above the glass transition temperature* (T_g); the segmental polymer relaxation rate is much faster than the solvent progress, and the solvent concentration increases from the non-affected polymer domains to the swollen regions, characterised by a constant spin–spin relaxation time (T_2). MRI was used to study the ingress of water into polyamide 6 at 100°C, and the results demonstrated that the diffusion follows Fick's law [2–4]. Studies of water in polycarbonates were also published [5]. Recently, MRI was used to observe water absorption by polymer electrolytes and the evidence for a Fickian diffusion mechanism were reported [6].

Solvent diffusion into amorphous polymers *below* T_g (glassy state) is described as a Case II behaviour, as the polymer secondary relaxations are much slower than the ingress of the solvent, and a sharp front, progressing at a rather constant velocity, separates the swollen polymer from the initial non-affected polymer; a decrease in the solvent T_2 relaxation rate towards the polymer core, is then obtained [7,8] and the formation of this front is fast.

Owing to the presence of hydrophilic sites, water uptake can be high and prolonged. The driving force for water uptake is the chemical potential gradient between the external water and the internal absorbed water droplets. The gradient will be larger for distilled water than for water containing salts and impurities, like ordinary water, leading to a higher water uptake.

Sodium polyacrylate (Na-Pa), $(-CH_2-CH(CO_2Na)-)_n$, a strong hydrophilic polymer, is able to absorb a volume of water several hundred times its own volume and, consequently, is widely applied as a super absorbent material. Evidence was obtained using Fourier transform infrared (FTIR) spectroscopy that divalent ions, like Zn^{2+}, can be chelated to the carboxylic groups of polyacrylate [9], thus forming salt-like bridges which may act as ionic cross-links between the polymer molecules [10]; such behaviour contrasts with that of monovalent ions, like Na^{+}, which seem not to be site bound but to remain labile in the swelled state [11].

We report here the study of water ingress into Na-Pa using MRI techniques which minimise the effects of strong magnetic susceptibility inhomogeneities that characterise

* Corresponding author. Tel.: +351-1-8418103; fax: +351-1-8418101.

0032-3861/00/$ - see front matter
PII: S0032-3861(99)00598-4

Table 1
Experimental conditions used for LF- and STRAFI-MRI data acquisition and corresponding resolutions along the 1-D projections

Parameter	LF-MRI	STRAFI-MRI
Static magnetic field, ^{1}H Frequency	0.1 T, 4.3 MHz	2.9 T, 123 MHz
Gradient	Pulsed, 5 mT/m	Static, 37.5 T/m
RF pulse sequence	$90°_x$–τ–$180°_y$–τ–echo	$[90°_x$–τ–$(90°_y$–τ–echo–$\tau)_n]$ with $n = 64$
90° pulse duration	600 μs	10 μs
Spin-echo time	8 ms	30 μs
Acquisition time	16 s (4 scans)	12 min (50 scans)
Linear resolution	≈ 1 mm	< 0.1 mm

the diffusion of liquids into porous media: MRI techniques using either very low static magnetic field (and low frequency-encoded gradient), LF-MRI [12], or high static magnetic field (and very high static magnetic field gradient), STRAFI-MRI [13], respectively. The STRAFI-MRI technique utilises the large static field gradients, present outside the central field region of a superconducting magnet. The image acquisition is performed with the application of an echo-sequence, in general a Powles–Mansfield sequence, of very short radiofrequency (RF)-pulses. Consequently, very short echo times can be achieved, allowing, for example, to study materials with strong magnetic susceptibility inhomogeneities, like Portland cement hydrating paste [14,15], or to obtain images of quadrupolar nuclei of half-integer spin [16].

In particular, STRAFI one-dimensional (1-D) profiles, which contain information on the undisturbed polymer as well as on the swollen region and the free water distribution, are compared with low-field data, clearly not containing information on the polymer.

2. Experimental

The Na-Pa sample used in these studies was received from Hoechst as a powder ($\bar{M}_w = 40 \times 10^6$ g mol^{-1}). The polymer was produced by reverse emulsion process and is mostly linear.

The ^{1}H 1-D images (profiles) were acquired, either with LF-MRI using a home-built whole body scanner, or with STRAFI-MRI using a Bruker MSL 300 P NMR spectrometer and a dedicated Bruker STRAFI probe. Glass containers with the appropriate cylindrical symmetry for 1-D observations were used, held vertically during the data acquisition. Their dimensions were: 40 mm height and 26 mm diameter, or 10 mm height and 10 mm diameter, for LF-MRI or STRAFI-MRI observations, respectively. Table 1 shows the experimental conditions selected for data acquisition and the linear resolutions achieved. Note that the nominal field intensity of the Bruker spectrometer (7.0 T) is reduced to 2.9 T in the optimum STRAFI region.

NMR spectroscopic studies were performed using a Bruker MSL 300 P spectrometer operating at 300.13, 75.47 and 79.15 MHz for ^{1}H, ^{13}C and ^{23}Na observations, respectively. The ^{1}H spectra were run with magic angle spinning (MAS) using a Hahn spin-echo RF-pulse sequence ($90°$–τ–$90°$–τ-signal acquisition), with a variable delay τ, in order to observe either a dominant contribution from protons in mobile parts of the sample ($\tau = 17$ μs), or to record also the signal from protons in more rigid domains ($\tau = 6$ μs). The pulse duration corresponding to a 90° magnetisation tip angle was 5.5 μs. A single RF-pulse sequence, with a pulse duration of 1.5 μs (equivalent to a 30° tip angle), was selected to run the ^{23}Na spectra and the standard CP/MAS technique (with proton decoupling) was used to observe the ^{13}C resonances (the pulse duration corresponding to a 90° tip angle was 5.1 μs). As external references (0 ppm)

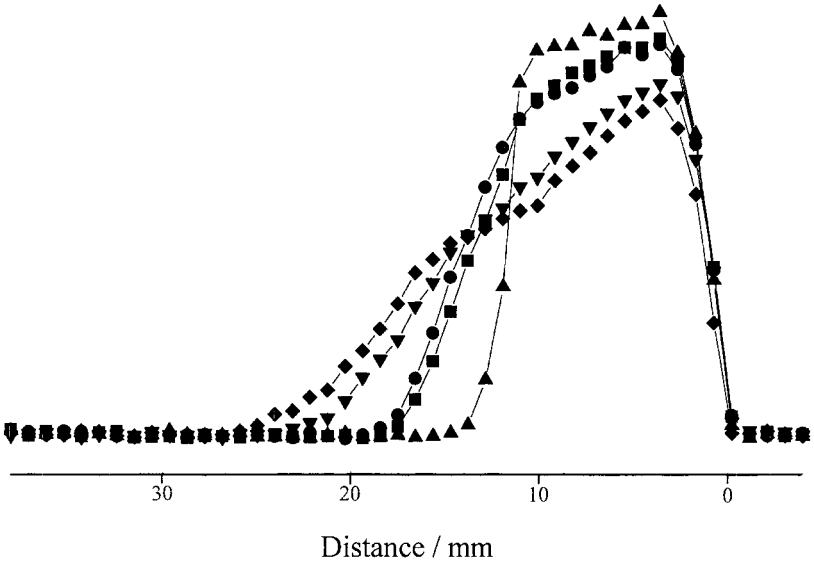

Fig. 1. 1-D projections obtained by LF-MRI from a cylindrical glass container, along the cylinder axis, partially filled with 6 g of water (up to 12 mm height) (▲), and at the following periods of time after adding 12 g of Na-Pa (reaching 35 mm height): (■) 3 min; (●) 44 min; (▼) 22 h and (◆) 44 h.

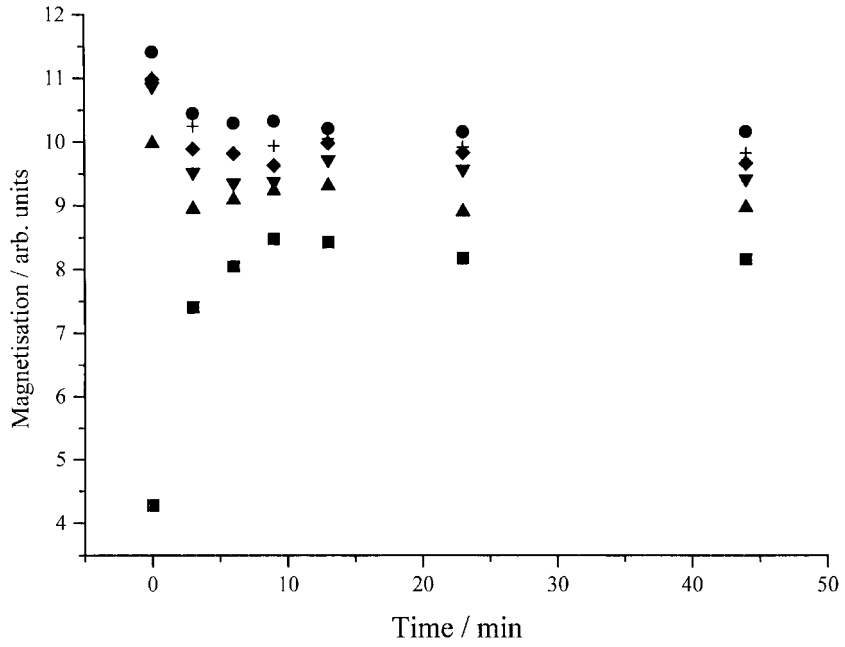

Fig. 2. Variation of the magnetisation (in arbitrary units) with time, obtained by LF-MRI over 50 min from the following slices: (●) close to the bottom of the container, (■) close to the water surface and (+◆▼▲) middle slices.

for ^{1}H, ^{13}C and ^{23}Na resonances, water, TMS and a saturated sodium chloride water solution were used, respectively.

3. Results and discussion

3.1. LF-MRI

Experiment 1. A cylindrical glass container, with the cylinder axis oriented perpendicularly to the main magnetic field, was partially filled with water (6g, up to 12 mm height) and a first 1-D profile was acquired (Fig. 1, triangles). Subsequently, 12 g of Na-Pa were added, which reached the height of 35 mm, and the acquisition of 1-D profiles was immediately started. The amounts of liquid and polymer in the container were such that, even after the sedimentation period, a large quantity of polymer was not in contact with the liquid. Fig. 1 shows the evolution with time of the 1-D profiles recorded over 44 h. The

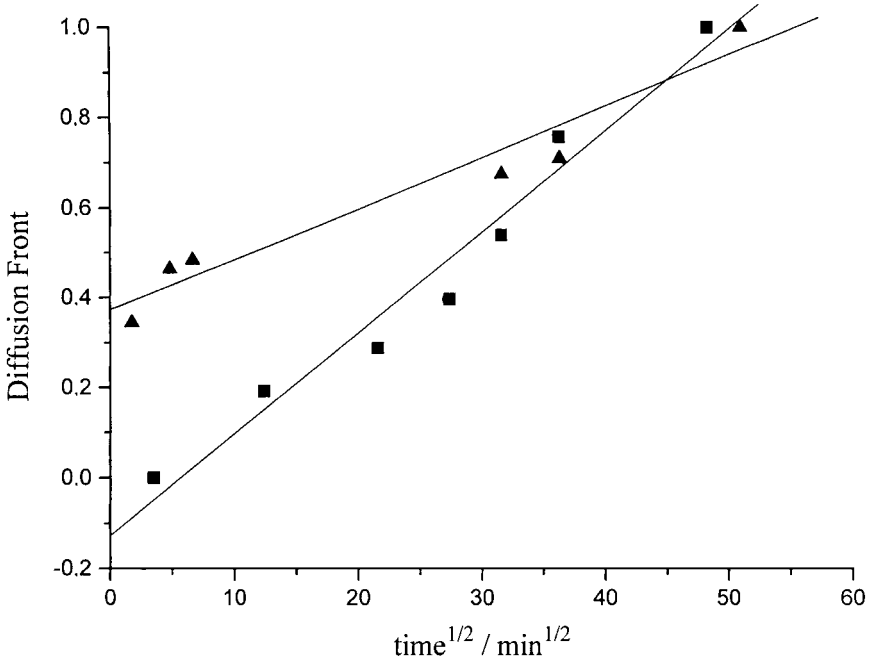

Fig. 3. Position of the water front versus the square root of time; data have been obtained either by LF-MRI (▲) or by STRAFI-MRI (■). Normalised values are displayed to enable a comparison of the results (see text for details). Plots of the linear functions used to fit the data are also shown.

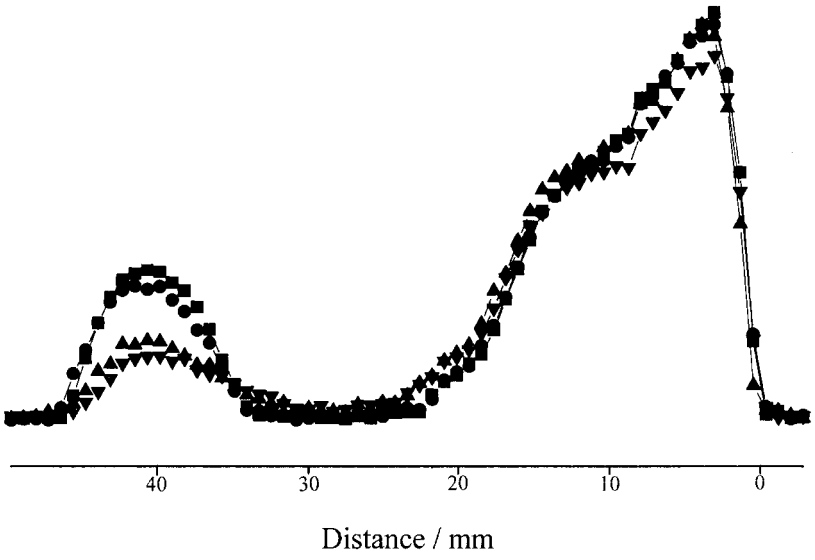

Fig. 4. Subsequent to Experiment 1 (see Fig. 1), 2 g of water was added on top of the polymer and 1-D projections were obtained by LF-MRI, at the following times after water addition: (■) immediately after; (●) 90 min; (▲) 18 h; and (▼) 22 h after.

integral of the signal along the profile remains constant within 2% over 44 h, which reveals that only signal from the initial water is observed, and no signal from the polymer was recorded. The water concentration decreases from the bottom toward the polymer core.

Fig. 2 shows the signal $S(t)$ obtained from different slices over 50 min. Data acquired from slices close to the bottom of the container can be fitted to $S(t) = S_1\exp(-t/t_0) + S_2$, where $S_1 + S_2$ is the original bulk water signal and S_2 the signal remaining after 50 min, t is the time after the polymer addition and t_0 is a characteristic time scale that mainly accounts for the polymer sedimentation period. We have obtained for t_0 about 2 min, comparable to the minimum delay between successive acquisitions, and for $S_1/(S_1 + S_2)$ about 90%, which means that the polymer volume fraction at the bottom of the container is about 10% after 50 min.

The position of the water front P, for each one of the profiles shown in Fig. 1, can be computed by interpolation as the position at half-maximum of a given profile. Fig. 3 (triangles) shows the normalised P values, using the P value obtained after 44 h as the normalisation factor, plotted versus $\sqrt{t}$; the data can be fitted to a linear function ($y = 0.37 + 0.01\sqrt{t}$), which shows that diffusion of water into NA-Pa follows a Case I behaviour.

T_2 profiles were also obtained from CPMG acquisitions with an echo spacing of 25 ms, and a mono exponential fit on 80 echoes. T_2-profiles were recorded after 24 h and 48 h (not shown): T_2 is approximately constant in the swollen region (650 ± 50 ms), but decreases from the solvent towards the polymer core. T_2 measured from the protons in the bulk distilled water is about 2000 ms in these experimental conditions. Water molecules being trapped in restricted domains, during the polymer swelling process and the consequent gel formation explain the observation of the proton T_2 decrease.

Experiment 2. Subsequent to Experiment 1, water (2 g) was added on the top of the polymer. The evolution of the profiles with time was recorded over 22 h (Fig. 4). This experiment gives additional evidence that the more rigid part of the polymer cannot be visualised in our experimental

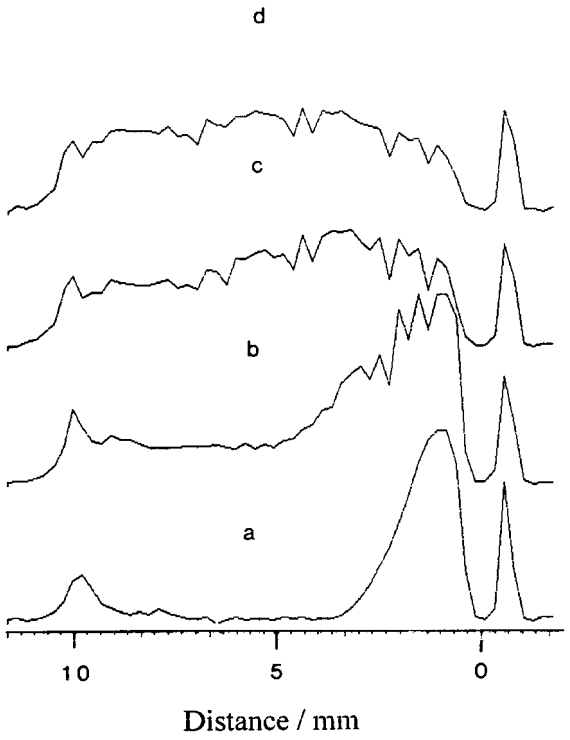

Fig. 5. Profiles obtained by STRAFI-MRI, from a cylindrical glass vial containing: (a) water and Na-Pa added to water; (b) 15 min; (c) 22 h; and (d) 39 h, after the addition of the polymer. The signal of a plastic disc used as a reference is shown on the right-hand side of the plots, also the bottom of the vial, and the signal of parafilm, used to cover the vial in order to avoid water evaporation, is observed on the left-hand side of the profiles.

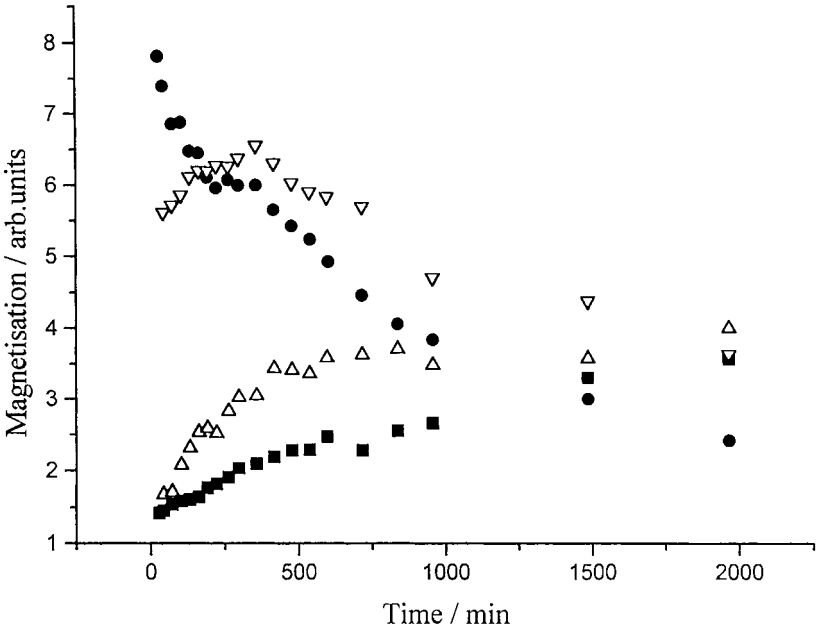

Fig. 6. Variation of the magnetisation, in arbitrary units, with time, obtained over 2000 min by STRAFI-MRI from the following slices at the indicated distances (mm) from the bottom of the sample: (●) 0.1; (▽) 2.4; (△) 4.3; and (■) 6.80.

conditions of LF-MRI. The decay of the water signal over 22 h, shown on top of Fig. 4, probably corresponds to water evaporation.

3.2. STRAFI-MRI

The experimental conditions used in STRAFI-MRI observations were similar to the ones described above for the LF-MRI Experiment 1, except for the dimensions of the container and for the amount of liquid (0.25 g) and polymer (1 g). The axis of the cylindrical vial was parallel to the main magnetic field direction, also the static magnetic field gradient direction. The 1-D projections obtained over 39 h are shown in Fig. 5. The integrals of the profiles (in arbitrary units, au) are as follows (assigning the value 1 au to the integral of the reference signal, shown on the right-hand side of the plots): Fig. 5(a), 6.7 au, obtained for the liquid, and Fig. 5(b)–(d) 19.0 ± 0.3 au, containing signals from the liquid and the polymer. A constant contribution of 12.3 au is thus obtained for the magnetisation recorded from the protons in the polymer. A constant hydrostatic pressure is reached inside the polymer after about 40 h, as determined by STRAFI-MRI (Fig. 5(d)).

Fig. 6 shows the variation of the magnetisation with time, obtained from the indicated slices. Mono-exponential functions fit the data acquired from a slice 0.09 mm from the bottom of the container. The functions $y = 5.6 + 1.9\exp(-(x - 42.5)/t_1)$ and $y = 1.9 + 3.9\exp(-(x - 403.9)/t_2)$ fit the data acquired from 15 to 250 min and from 300 to 2000 min, respectively; the time-constants t_1 and t_2 are 123 and 813 min, respectively. During the period 250–300 min the magnetisation remains constant.

From the profiles that are shown in Fig. 5, and also from other 1-D images recorded at different times (not shown), the position of the water front was computed as the interpolated value at half-maximum of each one of the profiles. These data, previously normalised using the value obtained after 44 h as the normalisation factor, are plotted on Fig. 3 (squares) versus $\sqrt{t}$; they better fit a $\sqrt{t}$ dependence ($y = -0.13 + 0.02\sqrt{t}$) than a t dependence. This brings to evidence that water diffusion into Na-Pa follows a Case I behaviour, consistently with LF-MRI data; moreover, taking into account that the polymer is not observed by LF-MRI and that the progress of the front is twice as fast as determined by STRAFI-MRI, we may conclude that STRAFI allows the observation of the swelling of the polymer (and the consequent gel formation) and that this process is about two times faster than the progress of the water front.

3.3. NMR spectroscopy

A ^{1}H spectrum of Na-Pa as-received (not shown) was obtained with an MAS rate of 4.2 kHz, using a single-RF pulse sequence and a pulse duration corresponding to a 45° magnetisation tip angle; one line with a full width at half maximum (FWHM) of 4.5 kHz was recorded. In the next step, a relaxation-weighted acquisition was performed, using the RF-pulse sequence mentioned in Section 2. Fig. 7(a) and (b) show, respectively, the ^{1}H spectra of Na-Pa as-received and over 40 h after the ingress of water into the polymer has started, that is, after the hydrostatic equilibrium was attained according to the STRAFI-MRI results; the spectra were obtained with an MAS rate of 5.2 kHz. Fig. 7(a) shows a broad signal at 0.06 ppm, with FWHM of

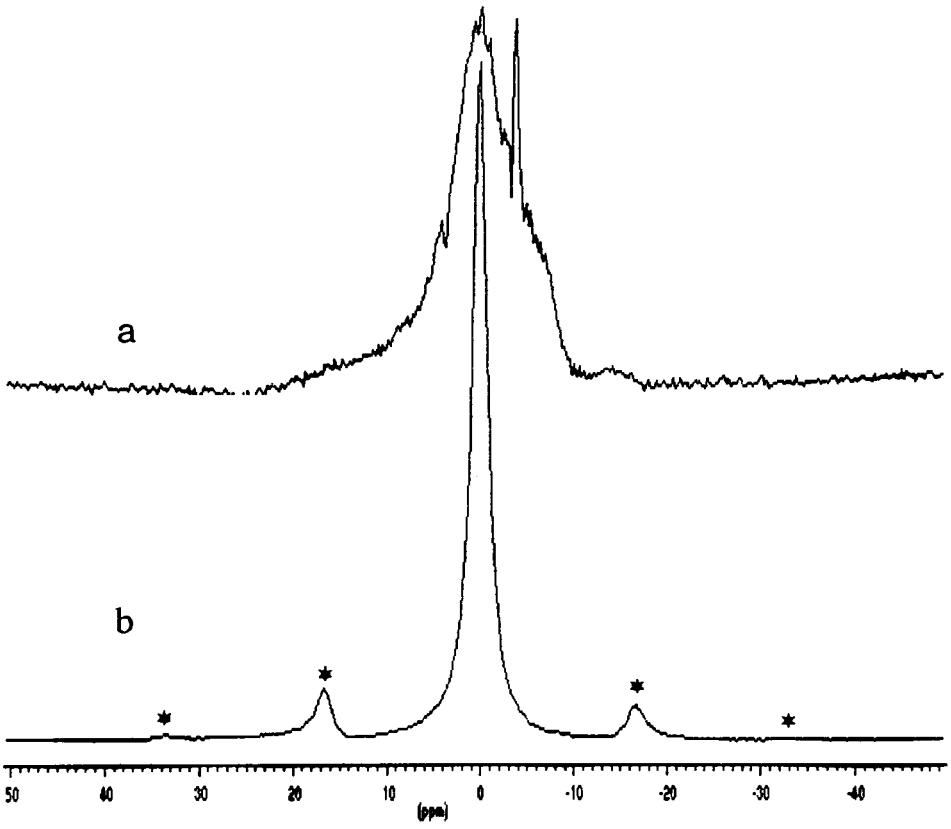

Fig. 7. ^{1}H NMR spectra obtained with a MAS rate of 5.2 kHz from Na-Pa as-received (a) and more than 40 h after the polymer water uptake has started (b).

2.5 kHz, and superimposed narrow signals (the most intense one observed at −3.8 ppm, with FWHM = 230 Hz), assigned to protons in the rigid backbone of Na-Pa (only detected in part, see Section 2 for details) and to protons in the polymer end groups and in water molecules absorbed from the surroundings, respectively.

Fig. 7(b) displays a centre line at 0.06 ppm with FWHM of 560 Hz and four spinning side bands. Using the intensities of these five lines as the input to the program masfit, based on the method of Herzfeld–Berger [17], we have obtained the principal components of the shielding anisotropy tensor: $\sigma_{11} = -2.47$ ppm, $\sigma_{22} = -2.32$ ppm and $\sigma_{33} = 4.97$ ppm. The chemical shift anisotropy, $\Delta\sigma = \sigma_{33} - (\sigma_{11} + \sigma_{22})/2$, and the asymmetry parameter, $\eta = (\sigma_{22} - \sigma_{11})/(\sigma_{33} - \sigma_{iso})$ were found to be 2.57 ppm and 0.03, respectively. The chemical shift tensor of the protons assigned to the line at 0.06 ppm is thus approximately axially symmetric, with a relatively small anisotropy. Taking into account that the HH distance, d_{HH}, in the methylene groups of the polymer is ca 17 nm, a dipolar coupling ($\mu_0 h\gamma^2 d_{HH}^{-3}/16\pi^3$, μ_0 is the vacuum permeability, h is the Planck's constant and γ is the proton nucleus magnetogyric ratio) of more than 20 kHz is obtained. At the MAS rate used for the proton spectrum acquisition, 5.2 kHz, it is not expected to obtain narrow lines unless the mobility of the polymer backbone increases and, consequently, a dipole–dipole line broadening is averaged out. However, the observation of an anisotropy of the chemical shift (2.57 ppm) is consistent with the presence of oriented polymer molecules. A decrease in the proton spectrum line width is also reported in the polymer electrolyte systems $Zn(CF_3SO_3)_2(PEO)_9$ and $Pb(CF_3SO_3)_2(PEO)_9$ following water uptake; the increased mobility induced by hydration was explained by the coordination of the cations by water molecules, not cross-linking the polymer chains [18,19].

The Na-Pa water uptake was also investigated observing the ^{23}Na resonances. A ^{23}Na nucleus (spin = 3/2) has an electric quadrupole moment that interacts with non-spherically symmetric (lower than tetrahedral symmetry) electric field gradients (EFG) generated at the nucleus by the surrounding atoms, leading to a broadening of the spectra. In general, MAS averages out the first-order interactions but the second-order interactions are not completely cancelled influencing mainly the central (−1/2,1/2) transition. In Na-Pa, the lone-pair electrons from the carboxylic group in Pa contribute to the EFG and consequently, the signal will be influenced by the mobility of either the sodium ions or the polymer chain.

The ^{23}Na spectra (not shown) were obtained with a MAS rate of 9 kHz. Before the ingress of water, an asymmetric line shape, showing a second-order quadrupolar effect, was recorded from Na-Pa (FWHM = 1.8 kHz, chemical shift = −16.3 ppm). This observation shows that the sodium atoms in Na-Pa are bonded to the polymer to be subjected to a non-spherically symmetric EFG. At the end of the water uptake,

a Lorentzian line shape, with no quadrupolar features, is observed for the sodium resonances (FWHM = 1.2 kHz, chemical shift = −6.6 ppm). This result is consistent with the sodium atoms in hydrated species, in which case the involvement of water molecules in intermolecular hydrogen bonds with Na-Pa carboxylic groups, leading to a gel structure, could explain the observation of the ^{23}Na signals shifted to a frequency lower than the one recorded for the ^{23}Na in hydrated sodium ions. In these species, the sodium ion is surrounded by water molecules as $Na(H_2O)_4^+$, in a symmetric tetrahedral environment, in which case the EFG at the nucleus is zero, and the chemical shift is 0 ppm [20]. Moreover, the present results rule out the formation of aggregated sodium ions, in view of the fact that ^{23}Na signals would be expected to be broad and asymmetric; aggregated sodium ions in sodium sulfonated polystyrene ionomers with a 4.2% sulfonation level were assigned to the ^{23}Na resonances observed at −17 ppm and the quadrupolar constant was calculated to be 1.6 MHz [21].

The ^{13}C spectra (not shown) were recorded with a MAS rate of 4 kHZ and a very short contact time (50 μs). This condition favours the observation of carbons other than the quaternary carbon atoms in rigid domains of the polymer. In the spectrum obtained from Na-Pa as-received, different signals, not well-resolved, with similar intensities, were observed in the range 20–50 ppm. A dominant signal was identified at 45 ppm in the spectrum of hydrated Na-Pa; this enhanced resonance is assigned to the carbons in CH groups close to the strongly oriented water molecules, giving rise to an additional ^{1}H–^{13}C magnetisation transfer.

4. Conclusions

The STRAFI-MRI results not only show that the Na-Pa hydration reaction follows a mono-exponential decay over the first five hours but also demonstrate that, after that period, the magnetisation decays primarily with a time-constant about one order of magnitude higher; this result is in agreement with the water molecules in two different environments and might be correlated with water in the open gel pore and in the capillary pore [22].

The exponential decays were fit to the experimental data obtained from slices at the bottom of the containers, either using LF-MRI or STRAFI-MRI techniques. The proton magnetisation obtained from these slices depends on sedimentation and swelling processes. Proton magnetisation acquired from slices near the surface is mainly governed by capillary and swelling processes.

It was shown that the water diffusion into Na-Pa follows a Fickian, Case I, behaviour and that the swelling of the polymer is about two times faster than the progress of the water front.

The complementarity of LF- and STRAFI-MRI techniques is clearly demonstrated in the study of Na-Pa water uptake. While LF-MRI provides *only the free water* resolved spatial distribution, using STRAFI-MRI, the magnetisation of *all the protons* in the sample, the protons in the free as well as in the bound water molecules and the protons in the polymeric backbone, is recorded. Nevertheless, using STRAFI-MRI, it is difficult to discriminate the protons in the free water molecules from those in other mobile species and the data acquisition time prevents the observation of fast hydration reactions. Susceptibility inhomogeneities, present in the Na-Pa gel, do not impose limitations to any of these techniques.

The ^{23}Na NMR data mainly show that all the sodium atoms are available for hydration and the recorded chemical shift is in agreement with the involvement of sodium coordinated water molecules in intermolecular bonds, giving rise to a gel structure. The measured ^{1}H chemical shift anisotropy indicates the presence of oriented polymer molecules. The ^{13}C results also point to the existence of short distances between the carbon atoms in the Na-Pa methine groups and the hydrogen atoms in the absorbed water molecules.

Acknowledgements

This work was supported on the frame of the CNRS/FCT co-operation and was also funded by the PRAXIS XXI Portuguese research programme (project PSAU/131/96).

References

[1] Alfrey T, Gurnee EF, Lloyd WG. J Polym Sci Part C 1966;12:249.
[2] Blackband S, Mansfield P. J Phys C: Solid State Phys 1986;19:L49.
[3] Mansfield P, Bowtell R, Blackband S. J Magn Res 1992;99:507.
[4] Fyfe CA, Randall LH, Burlinson NE. J Polym Sci A: Polym Chem 1993;31:159.
[5] Fyfe CA, Randall LH, Burlinson NE. Chem Mater 1992;4:267.
[6] Lauenstein A, Tegenfelt J, Kuhn W. Macromolecules 1998;31:3886.
[7] Ercken M, Adriaensens P, Vanderzande D, Gelan J. Macromolecules 1995;28:8541.
[8] Weisenberg LA, Koenig JL. Macromolecules 1990;23:2445.
[9] Nicholson JW, Brookman PJ, Lacy OM, Sayers GS, Wilson AD. J Biomed Mat Res 1988;22:623.
[10] Wall FT, Drennan JW. J Polym Sci 1951;7:83.
[11] Nicholson JW, Wasson EA, Wilson AD. Br Polym J 1988;20:97.
[12] Guillot G, Dupas A. In: Colombet P, Grimmer AR, editors. Application of NMR spectroscopy to cement science, New York: Gordon and Breach, 1994. p. 313.
[13] Samoilenko AA, Artemov DY, Sibeldina LA. JETP Lett 1988;47:417.
[14] Nunes T, Bodart P, Randall EW, Samoilenko AA, Feio G. J Phys D: Appl Phys 1996;29:805.
[15] Nunes T, Bodart P, Randall EW. In: Colombet P, Zanni H, editors. Proceedings of the second international conference on NMR spectroscopy of cement based materials, Berlin: Springer, 1997.
[16] Bodart P, Nunes T, Randall EW. Solid State NMR 1997;8:257.
[17] Herzfeld J, Berger AE. J Chem Phys 1980;73:6021.
[18] Lauenstein A, Johansson A, Tegenfelt J. J Electrochem Soc 1994;141:1819.
[19] Johansson A, Lauenstein A, Tegenfelt J. J Phys Chem 1995;99:6163.
[20] Komoroski RA, Mauritz KA. J Am Chem Soc 1978;100:7487.
[21] O'Connel E, Thatcher WR, Cooper SL. Macromolecules 1994;27:5803.
[22] Halperin WD, Jehng J-Y, Sung Y-O. Magn Reson Imaging 1994;12:169.